Research Square

Preprints are preliminary reports that have not undergone peer review.
They should not be considered conclusive, used to inform clinical practice,
or referenced by the media as validated information.

Chemical characterization and pH-responsive optical behavior of a cold atmospheric plasma-pretreated Punica granatum var. pleniflora extract

Mohammad Abdollahpour
Islamic Azad University
Farid Amidi-Fazli
amidif@iau.ac.ir

Islamic Azad University
Jalal Shayegh
Islamic Azad University
Mehdi Gharekhani
Islamic Azad University
Ali Rezapour
Islamic Azad University

Research Article

Keywords: Punica granatum, cold atmospheric plasma, GC–MS, pH-responsive color, UV–Vis spectroscopy, digital image colorimetry

Posted Date: November 13th, 2026

DOI: https://doi.org/10.21203/rs.3.rs-11482323/v1

License: This work is licensed under a Creative Commons Attribution 4.0 International License.
Read Full License

Additional Declarations: No competing interests reported.

Chemical characterization and pH-responsive optical behavior of a cold atmospheric plasma-pretreated *Punica granatum* var. *pleniflora* extract

Mohammad Abdollahpour[a], Farid Amidi-Fazli[b,c]*, Jalal Shayegh[d*], Mehdi Gharekhani[a], Ali Rezapour[e]

[a] Department of Food Science and Technology, Ta.C., Islamic Azad University, Tabriz, Iran
m.gharekhani@iau.ac.ir
[b] Department of Food Science and Technology, Sou.C., Islamic Azad University, Soufian, Iran
amidif@iau.ac.ir
[c] Industrial Nanotechnology Research Center, Ta.C., Islamic Azad University, Tabriz, Iran
[d] Department of Veterinary Medicine, Shab.C., Islamic Azad University, Shabestar, Iran
jalalshayegh@iau.ac.ir
[e] Department of Animal Science, Ta.C., Islamic Azad University, Tabriz, Iran
ali.rezapour@iau.ac.ir
*Corresponding Author: Farid Amidi-Fazli
ORCID: 0000-0002-3482-9322
*Corresponding Author: Jalal Shayegh
ORCID: 0000-0003-2606-3168Q2

Abstract

Cold atmospheric plasma (CAP) pretreatment can modify the chemical characteristics of plant extracts and may influence their functional and optical properties. This study investigated the chemical composition and pH-dependent optical behavior of a CAP-pretreated extract of *Punica granatum* var. *pleniflora*. The extract obtained under the previously selected CAP treatment condition was compared with an untreated control and subsequently characterized by GC–MS, digital image color analysis, and UV–Vis spectroscopy across pH 2–12. CAP pretreatment significantly altered several extract characteristics, including extraction yield, ferric-reducing antioxidant power, total phenolic content, and anthocyanin content, whereas changes in DPPH activity and flavonoids were not statistically significant. GC–MS provided tentative annotations of diverse chemical constituents, with phenolic/aromatic, furanic, and fatty-acid compounds among the major classes. The extract exhibited pronounced pH-dependent changes in CIELAB color parameters, with a major optical transition around the neutral region, a relatively stable darker state at pH 8–11, and a further distinct response at pH 12. Corresponding changes in visible absorption were observed by UV–Vis spectroscopy. Integrated PCA of colorimetric and spectral descriptors explained 96.64% of the total variance within the first two components. The combined chemical, colorimetric, and spectroscopic results demonstrate a systematic pH-responsive optical behavior of the extract and support its further investigation as a natural pH-responsive colorant or sensing component.

Keywords: *Punica granatum*; cold atmospheric plasma; GC–MS; pH-responsive color; UV–Vis spectroscopy; digital image colorimetry

1. Introduction

Punica granatum L., commonly known as pomegranate, is an ancient fruit crop belonging to the family Lythraceae that has been cultivated for millennia across the Mediterranean, Middle East, and parts of Asia. Beyond its culinary appeal, pomegranate has gained substantial scientific and commercial interest because of its exceptionally rich profile of bioactive secondary metabolites. The fruit (arils, peel, and seeds) contains high concentrations of hydrolysable ellagitannins—principally punicalagin (α- and β-anomers) and ellagic acid—along with flavonoids, phenolic acids (gallic acid, caffeic acid), and a distinctive suite of anthocyanins, primarily cyanidin, delphinidin, and pelargonidin glycosides. These compounds collectively confer potent antioxidant, anti-inflammatory, antimicrobial, cardioprotective, antidiabetic, and anticancer activities. Punicalagin, in particular, has been shown to modulate multiple cellular signaling cascades, including Nrf2/HO-1, AMPK, NF-κB, PI3K/AKT, and MAPK pathways, thereby reducing oxidative stress, suppressing pro-inflammatory cytokines, improving endothelial function, and influencing lipid metabolism. Clinical and preclinical evidence further supports beneficial effects on cardiovascular risk markers, glycemic control, and gut microbiota-derived urolithins, underscoring the value of pomegranate extracts as functional food ingredients and nutraceutical candidates (Cheng et al. 2023; Maqsood et al. 2025; Zhang et al. 2025).

Efficient recovery of these heat- and oxygen-sensitive phytochemicals remains a technological challenge. Conventional solid–liquid extraction typically employs hydroalcoholic solvents (often ethanol–water mixtures) under elevated temperatures or prolonged contact times. While effective to a degree, such processes can degrade labile anthocyanins and ellagitannins, promote oxidative polymerization, consume large volumes of solvent, and generate substantial energy and environmental costs. Consequently, non-thermal "green" extraction technologies have attracted increasing attention. Among these, cold atmospheric plasma (CAP)—also termed cold plasma or non-thermal plasma—has emerged as a versatile pretreatment and processing tool. CAP is generated by applying an electric field to a gas (air, argon, nitrogen, or mixtures) at or near atmospheric pressure, producing a partially ionized medium rich in reactive oxygen and nitrogen species (RONS: O, OH•, O_3, NO•, NO_2, etc.), ultraviolet photons, electrons, ions, and electric fields, while the bulk gas temperature remains close to ambient (Heydari et al. 2023).

The interaction of these reactive species with plant matrices induces several synergistic effects that facilitate extraction. Physical etching and ablation create micro-cracks, pores, and increased surface roughness, thereby enlarging the effective surface area available for solvent contact. Chemical oxidation and depolymerization of cell-wall polysaccharides (cellulose, hemicellulose, pectin) and cuticular waxes weaken structural barriers and enhance hydrophilicity, promoting solvent penetration and the release of intracellular metabolites. In some systems, mild oxidative stress may also trigger secondary metabolic responses that elevate the pool of extractable phenolics. Importantly, because bulk temperatures remain low, thermal degradation of thermolabile compounds is minimized (Heydari et al. 2023).

Empirical evidence supporting CAP-assisted extraction of polyphenols is growing rapidly. Enhancements have been reported for tomato pomace(Bao et al. 2020), green tea leaves(Keshavarzi et al. 2020), hyssop (Ahmadian et al. 2023), clove (Alashti et al. 2023), spent coffee grounds (Kyriakoudi et al. 2024), where CAP pretreatments of only a few minutes elevated total phenolic content (TPC), total flavonoid content (TFC), and radical-scavenging activity. With respect to pomegranate specifically, pioneering studies demonstrated that cold atmospheric gas-phase plasma applied to juice increased total anthocyanin content by 21–35 % under optimized conditions (short exposure, moderate argon flow) while modulating color parameters (Bursać Kovačević et al. 2016). Parallel work showed a ~33 % rise in total phenolic content relative to untreated juice, with plasma performance comparable or superior to thermal pasteurization (Herceg et al. 2016). More recent investigations on solid matrices—pomegranate peels, seed meal obtained by cold pressing, and pomace powder—have confirmed that CAP pretreatments (dielectric-barrier discharge or multipin atmospheric systems, voltages typically 15–35 kV, times 5–30 min) can significantly elevate TPC and TFC, enhance DPPH and FRAP values, alter surface morphology (SEM-verified disruption), reduce antinutritional factors, and preserve or improve color stability (Ghasemi-Nezhad et al. 2025).

Anthocyanins, the pigments responsible for the vivid red-to-purple coloration of pomegranate arils and extracts, exhibit a uniquely complex, pH-dependent chemistry that is central both to their visual properties and to their analytical characterization(Salim et al. 2023). In aqueous solution, anthocyanins exist as a multistate system of interconvertible species (Shu et al. 2026). Under strongly acidic conditions (pH ≈ 1–3) the red flavylium cation (AH^+) predominates and absorbs maximally around 510–530 nm. As pH rises, rapid deprotonation yields the purple quinoidal base (A) and, at still higher pH, the blue anionic quinoidal form (A^-). Concurrently, nucleophilic addition of water at C-2 generates the colorless carbinol (hemiketal) pseudobase (B), which undergoes ring-opening tautomerization to pale-yellow cis- and trans-chalcones (Cc, Ct). Above approximately pH 7–8 the equilibrium strongly favors the colorless or faintly yellow forms, resulting in progressive loss of visible color. These reversible structural transformations produce characteristic shifts in UV–Vis absorption spectra across the 190–800 nm window and give rise to the well-documented color changes observed when pomegranate extracts are adjusted across the pH range 2–12. Spectrophotometric monitoring of these changes, coupled with quantitative colorimetry, therefore provides a sensitive probe of anthocyanin integrity and of the broader phenolic environment, including possible copigmentation or degradation products induced by plasma treatment(Ahmed et al. 2026).

Complementary chemical profiling by gas chromatography–mass spectrometry (GC–MS) supplies structural identification of volatile and semi-volatile constituents—organic acids, phenolic derivatives, fatty-acid methyl esters (Fontana et al. 2018; Sun et al. 2023), and potential plasma-generated transformation products—thereby linking macroscopic antioxidant metrics to molecular composition (Kumar et al. 2024; Razazian et al. 2026). When these spectroscopic and chromatographic data are integrated with classical assays of extraction yield, TPC (Folin–Ciocalteu), TFC, total monomeric anthocyanins (pH-differential method), DPPH radical-scavenging activity, and ferric-reducing antioxidant power (FRAP), a multidimensional picture of CAP efficacy emerges.

Despite the expanding literature on CAP applications to pomegranate juice and by-products, systematic comparisons of CAP-pretreated solid plant material versus untreated controls under standardized hydroalcoholic extraction (70:30 ethanol–water), followed by exhaustive characterization of the resulting dry extracts with respect to antioxidant capacity, pH-dependent spectroscopic and colorimetric behavior, and GC–MS chemical profiles, remain limited. The present study addresses this gap. Punica granatum material was subjected to CAP pretreatment at defined conditions (20 min, 50 W) and compared with an untreated control. The overarching aim is to quantify the impact of CAP pretreatment on bioactive recovery and antioxidant performance, to correlate these quantitative changes with pH-dependent spectroscopic signatures, and to interpret the observed differences in light of the molecular profile revealed by GC–MS. The results are expected to advance the rational design of plasma-assisted green extraction protocols for high-value *Punica granatum* var. *pleniflora* extracts destined for functional-food and nutraceutical applications.

2. Materials and Methods

2.1. Materials and Reagents

Punica granatum var. *pleniflora* was sourced from Giah Kala Company (Iran). Ethanol (Extra Pure) was purchased from Merck (Germany). Folin–Ciocalteu's phenol reagent and sodium carbonate were obtained from Merck (Germany). Gallic acid (97.5–102.5%, titration) and quercetin were supplied by Sigma-Aldrich (USA). 2,2-Diphenyl-1-picrylhydrazyl (DPPH) was purchased from Sigma (D9132, USA). Aluminum chloride, potassium acetate, and dimethyl sulfoxide (DMSO) were acquired from Merck (Germany). Gentamycin and ketoconazole were provided by Padtan Teb Company (Iran). All buffers were prepared using analytical-grade chemicals from Merck (Germany). All reagents were of analytical grade unless otherwise stated.

2.2. Cold Plasma Pretreatment

Five grams of ground *Punica granatum* var. *pleniflora* material were placed on a sample holder inside a vacuum chamber. The chamber pressure was reduced to 0.15 Pa and then filled with artificial atmospheric air. Cold plasma was generated by applying a voltage of 120 V between two electrodes positioned 13 cm apart. Treatments were performed at power 50 W for 20 min. An untreated sample (0 min, 0 W) served as the control.

2.3. Extraction Procedure and Extraction Yield

The plant material was ground using a laboratory mill (IKA, MultiDrive control BT package, Germany). For extraction, 5 g of powder was mixed with 100 mL of 70% (v/v) hydroalcoholic ethanol and shaken for 24 h at room temperature. The mixture was filtered through Whatman No. 42 filter paper. The solvent was evaporated using a rotary evaporator (Büchi, model B-480, Switzerland) at 60°C and 20 rpm, followed by final drying in an oven (Memmert, model UF-55, Germany) at 40°C. The dried extract was stored in dark containers

at refrigeration temperature (Khalili et al. 2025). All extractions were performed in triplicate. Extraction yield was calculated as:

$$Extraction\ yield\ (\%) = \frac{weight\ of\ dried\ extract}{weight\ of\ initial\ dry\ plant\ powder} \times 100 \quad (1)$$

2.4. Chemical analysis

2.4.1. Determination of Total Phenolic Content

Total phenolic content was determined by the Folin–Ciocalteu method (Singleton and Rossi 1965). Briefly, 0.1 g of dried extract was dissolved in ethanol to a final volume of 100 mL. Then, 0.5 mL of this solution was mixed with 0.5 mL of 10% Folin–Ciocalteu reagent. After 5 min, 2 mL of 7.5% sodium carbonate was added. The mixture was incubated for 2 h at room temperature, and absorbance was measured at 760 nm using a spectrophotometer (Hach, UV-Vis DR5000, USA). Results were expressed as mg gallic acid equivalents per gram of extract.

2.4.2. DPPH Radical Scavenging Activity

DPPH free radical scavenging activity was measured according to Shimada et al. (1992). One hundred microliters of extract solution were mixed with 3.9 mL of 100 µM methanolic DPPH solution and incubated in the dark for 30 min. Absorbance was read at 517 nm (Hach, UV-Vis DR5000, USA) (Shimada et al. 1992). The percentage inhibition was calculated as:

$$I = \frac{Ac - As}{Ac} \times 100 \quad (2)$$

Where: (I): Percentage of free radical inhibition, (Ac): Absorbance of the control, and (As): Absorbance of the sample

2.4.3. Ferric Reducing Antioxidant Power (FRAP)

FRAP assay was performed according to (Benzie and Strain 1996). Fifty milligrams of dried extract were dissolved in 50 mL hydroalcoholic solvent. Then, 0.2 mL of this solution was mixed with 1.8 mL of FRAP reagent and incubated at 37°C for 10 min. Absorbance was measured at 593 nm using a spectrophotometer (Hach, UV-Vis DR5000, USA).

2.4.4. Total Flavonoid Content

Total flavonoid content was determined using the aluminum chloride colorimetric method (Chang et al. 2002). Briefly, 0.5 mL of extract solution was mixed with 0.5 mL of 10% aluminum chloride, 0.1 mL of 1 M potassium acetate, and 2.8 mL distilled water. After 30 min incubation at room temperature, absorbance was measured at 415 nm. Results were expressed as mg quercetin equivalents per gram of extract.

2.4.5. Total Anthocyanin Content

Total monomeric anthocyanin content was determined by the pH-differential method (Belwal et al. 2016). One hundred microliters of extract were mixed separately with 1.5 mL of potassium chloride buffer (0.025 M, pH 1.0) and sodium acetate buffer (0.4 M, pH 4.5). Absorbance was measured at 520 nm and 700 nm. The absorbance difference (A) was calculated as:

$$\text{Anthocyanin} = \frac{A \times Mw \times DF \times V \times 1000}{m \times l \times 26900} \quad (3)$$

$$A = (A_{520}-A_{700})_{pH1.0} - (A_{520}-A_{700})_{pH4.5} \quad (4)$$

Where MW = 449.2 g/mol (cyanidin-3-glucoside), DF = dilution factor, m = sample weight (g), and l = path length (cm).

2.5. Identification of Chemical Compounds (GC-MS Analysis)

The chemical composition of the untreated and plasma-treated *Punica granatum* var. *pleniflora* extracts was analyzed using gas chromatography-mass spectrometry (GC-MS). An Agilent 7890B gas chromatograph coupled with a 5977A mass spectrometer was employed, equipped with a split/splitless injector and electron ionization (EI) source. Separation was carried out on an HP-5MS capillary column (60 m × 0.25 mm i.d., 0.25 µm film thickness). The injector, interface, and ion source temperatures were set at 270°C, 250°C, and 230°C, respectively. The oven temperature program was as follows: 70°C (held for 3 min), ramped at 10°C/min to 180°C (held for 2 min), then ramped at 20°C/min to 295°C (held for 5 min). The split ratio was 1:20, and the injection volume was 0.5 µL. Mass spectra were acquired in scan mode and compared with NIST and Wiley libraries for compound identification.

2.6. pH-dependent color analysis and UV–Vis spectroscopy

The optical behavior of the selected SWE extract was evaluated over the pH range of 2–12. The pH of the solutions was adjusted using 0.2 M disodium hydrogen phosphate, 0.2 M citric acid, and 0.2 M sodium hydroxide solutions in different proportions (Yang et al. 2021).

2.6.1. Digital image acquisition and CIELAB color analysis

Color measurements were performed using a standardized digital imaging procedure. A custom black box was used to minimize variations in the imaging environment, and a white reference background was included during image acquisition. Samples were positioned at a fixed distance of 10 cm from the camera. Images were acquired using a Canon IXY 10S digital camera (16 megapixels, Japan) under identical camera settings, sample positioning, illumination conditions, and imaging distance for all pH levels.

The acquired images were analyzed using ImageJ software (National Institutes of Health, Bethesda, MD, USA). Mean RGB values were obtained from selected regions of each sample and converted to the CIELAB color space. The resulting color parameters included lightness (L*), red–green coordinate (a*), yellow–blue coordinate (b*), chroma (C*), and hue angle (h°). Chroma was calculated according to Eq. (5):

$$C^* = \sqrt{(a^*)^2 + (b^*)^2} \quad (5)$$

The hue angle was calculated from the CIELAB coordinates using the two-argument arctangent function according to Eq. (6):

$$h^\circ = \text{atan2}(b^*, a^*) \times \frac{180}{\pi} \quad (6)$$

When the resulting angle was negative, 360° was added to obtain a hue angle within the range of 0–360°. This quadrant-aware calculation was used to ensure consistent assignment of hue angle across the complete CIELAB a*–b* coordinate plane.

The total color difference (ΔE*) between each pH-adjusted sample and the pH 7 reference solution was calculated according to Eq. (7):

$$\Delta E^* = \sqrt{(L^* - L_7^*)^2 + (a^* - a_7^*)^2 + (b^* - b_7^*)^2} \quad (7)$$

where L_7^*, a_7^*, and b_7^*represent the CIELAB coordinates of the pH 7 reference solution, and L^*, a^*, and b^*represent the corresponding coordinates of each pH-adjusted sample.

The color parameters and calculation procedures were based on established CIELAB color relationships, with the hue calculation explicitly implemented using a quadrant-aware formulation to avoid ambiguity associated with the single-argument arctangent function. Similar CIELAB color measurements have been applied in recent studies of plant extracts, including butterfly pea extracts (Altaf and Intipunya 2026).

2.6.2. UV–Vis spectroscopy

UV–Vis spectra of the pH-adjusted extract solutions were recorded using a Hach DR5000 UV–Vis spectrophotometer (USA). Distilled water was used as the blank. Absorbance spectra were initially recorded over the wavelength range of 190–800 nm. The 250–450 nm region was subsequently selected for detailed spectral analysis.

The spectral descriptors included maximum absorbance ($A_{\max}$), wavelength of maximum absorbance ($\lambda_{\max}$), integrated absorbance over 250–450 nm, and spectral centroid. These descriptors were used to characterize changes in the absorption profile associated with pH.

2.7. Statistical Analysis

All statistical analyses were performed using R software (R version 4.5.1; RStudio version 2025.05.1+513). Experimental results obtained from triplicate measurements were expressed as mean ± standard deviation (SD). For comparison of the untreated control and cold atmospheric plasma (CAP)-pretreated extracts, differences between the two groups were evaluated using Welch's two-sample *t*-test, which does not assume equal variances. Percentage changes relative to the control were calculated to facilitate interpretation of the magnitude and direction of the treatment effects. Statistical significance was considered at $p < 0.05$.

Principal component analysis (PCA) was subsequently performed to integrate the colorimetric and spectroscopic measurements. For PCA, the mean color values at each pH were combined with the corresponding integrated spectral areas. Variables were centered and standardized before PCA. Chroma (C*) and ΔE were excluded because they are mathematically derived from the CIELAB coordinates, while individual spectral wavelengths and spectral PCA scores were excluded to minimize redundancy. The first two principal components were used to visualize the major patterns in the integrated optical response.

3. Results and discussion

3.1. Control and CAP-pretreated extracts: changes in chemical and functional characteristics

A preliminary comparison was performed between the untreated control and CAP-pretreated extracts to establish the overall changes associated with the pretreatment before investigating the chemical composition and pH-dependent optical behavior of the selected extract. As shown in Table 1, CAP pretreatment did not uniformly enhance all extraction responses; rather, it produced a distinct pattern of changes in extraction yield, antioxidant capacity, and phytochemical contents.

The extraction yield decreased significantly from 29.84 ± 1.32% in the control extract to 20.58 ± 1.09% following CAP pretreatment, corresponding to a 31.04% reduction ($p = 0.0008$). In contrast, FRAP increased from 2270.86 ± 91.08 to 2724.71 ± 119.77, representing a 19.99% increase ($p = 0.0077$). Thus, the CAP-treated sample cannot be considered simply a higher-yield extract. Instead, the contrasting responses suggest that pretreatment altered the composition of the material recovered during extraction and/or the relative contribution of different compounds to the measured antioxidant properties.

TPC decreased significantly after CAP pretreatment, from 19,837.89 ± 906.25 to 17,527.46 ± 680.47 mg GAE/100 g ($p = 0.0274$), while anthocyanin content decreased from 15,392.38 ± 508.47 to 13,515.48 ± 613.04 mg/100 g ($p = 0.0161$). Conversely, flavonoid content increased from 1874.08 ± 102.73 to 2053.59 ± 52.84 mg/100 g, although the difference was not statistically significant ($p = 0.0746$). DPPH radical-scavenging activity showed a similar numerical increase from 79.02 ± 2.21 to 85.15 ± 3.27%, but this difference also did not reach statistical significance ($p = 0.0630$).

The apparently contrasting behavior of total phenolic content and antioxidant capacity is noteworthy. Total phenolic assays provide a global estimate of compounds capable of reacting with the assay reagent, whereas antioxidant assays reflect the combined reducing or radical-scavenging behavior of the extract matrix. Consequently, changes in individual phenolic composition, relative abundance, accessibility, or the contribution of non-phenolic antioxidant constituents can result in different trends among TPC and antioxidant measurements (Fischer et al. 2013; Turfan et al. 2011). The present data therefore indicate a compositional modification rather than a generalized improvement in extract quality.

Table 1. Comparison of the chemical and antioxidant characteristics of control and CAP-pretreated *Punica granatum* var. *pleniflora* extracts.*

Response	Control	CAP	Change (%)	*p*-value
DPPH	79.02 ± 2.21	85.15 ± 3.27	+7.75	0.063
Extraction yield	29.84 ± 1.32	20.58 ± 1.09	−31.04	<0.001
FRAP	2270.86 ± 91.08	2724.71 ± 119.77	+19.99	0.008
TPC	19837.89 ± 906.25	17527.46 ± 680.47	−11.65	0.027
Flavonoids	1874.08 ± 102.73	2053.59 ± 52.84	+9.58	0.075
Anthocyanins	15392.38 ± 508.47	13515.48 ± 613.04	−12.19	0.016

*Values are presented as mean ± SD (n = 3). Percentage change was calculated relative to the control. p-values were obtained using Welch's two-sample t-test; $p < 0.05$ was considered statistically significant. CAP, cold atmospheric plasma; DPPH, 2,2-diphenyl-1-picrylhydrazyl radical-scavenging activity; FRAP, ferric-reducing antioxidant power; TPC, total phenolic content.

CAP pretreatment significantly modified several characteristics of the Punica granatum var. pleniflora extract, decreasing extraction yield, TPC, and anthocyanin content while increasing FRAP. DPPH activity and flavonoid content also increased numerically but were not statistically significant under the present small-sample comparison. This differentiated response provided the rationale for further characterization of the CAP-pretreated extract. In particular, GC–MS analysis was used to provide a broad chemical profile, while subsequent colorimetric and UV–Vis analyses were used to investigate whether the resulting extract exhibited a systematic pH-dependent optical response.

3.2. Chemical profile of the CAP-pretreated extract by GC–MS

GC–MS analysis provided a broad chemical profile of the CAP-pretreated Punica granatum var. pleniflora extract and revealed a chemically diverse matrix comprising phenolic/aromatic compounds, furanic and other oxygenated compounds, fatty acids and fatty-acid esters, carbohydrates, and several minor chemical classes (Table 2; Supplementary Table S1). Because the compound assignments were primarily based on mass-spectral library matching rather than confirmation with authentic standards, the reported compounds are considered tentative annotations. This distinction is important because library matching can provide useful structural candidates, but definitive compound identification generally requires additional evidence, such as comparison with an authentic standard under comparable analytical conditions.

The largest individual chromatographic annotation was 1,2,3-benzenetriol, which accounted for 22.65% of the selected relative peak area. 5-Hydroxymethylfurfural (HMF) represented the second-largest annotation (12.94%), followed by n-hexadecanoic acid (12.79%) and 9,12-octadecadienoic acid (Z,Z)- (11.96%). At the chemical-class level, fatty acids represented 29.50% of the classified relative peak area, while phenolic/aromatic and furanic compounds represented 24.21% and 18.71%, respectively. Thus, these three classes

together accounted for approximately 72.4% of the classified relative peak area and constituted the principal features of the chemical profile.

The prominence of the phenolic/aromatic fraction is consistent with the recognized complexity of Punica granatum var. pleniflora phytochemistry, in which phenolic compounds occur alongside anthocyanins and other classes of secondary metabolites. The presence of 1,2,3-benzenetriol as the largest library annotation should nevertheless be interpreted cautiously because the GC–MS library assignment does not by itself establish its absolute identity or quantitative concentration. Its high relative peak area indicates that a compound producing a closely matching mass spectrum was a major chromatographic component, rather than providing definitive evidence that this particular structure accounts for the entire peak.

The furanic fraction was also notable, particularly because HMF accounted for 12.94% of the selected relative peak area and additional furanic annotations included 3-furaldehyde, 5-methylfurfural, and 2,5-furandicarboxaldehyde. The occurrence of these compounds is compatible with the presence of processing-related oxygenated products in a plant extract subjected to extraction and pretreatment conditions (Reisdorph et al. 2019; Zulfiqar et al. 2023) . However, the present experiment does not include a paired GC–MS comparison demonstrating changes in these compounds between the untreated and CAP-pretreated samples. Therefore, their presence should be described as chemical context for the treated extract rather than as direct evidence that CAP generated these compounds.

Table 2. Major and chemically relevant compounds tentatively annotated by GC–MS in the CAP-pretreated *Punica granatum* var. *pleniflora* extract.*

No.	Tentatively identified compound	RT (min)	Relative peak area (%)	Chemical class
1	1,2,3-Benzenetriol	16.169	22.654	Phenolic/aromatic
2	5-Hydroxymethylfurfural	14.114	12.937	Furanic
3	n-Hexadecanoic acid	22.906	12.789	Fatty acid
4	9,12-Octadecadienoic acid (Z,Z)-	24.210	11.960	Fatty acid
5	D-Allose	17.842	5.875	Carbohydrate-related
6	3-Furaldehyde	5.920	2.782	Furanic
7	Octadecanoic acid	24.370	2.773	Fatty acid
8	4H-Pyran-4-one, 2,3-dihydro-3,5-dihydroxy-6-methyl-	12.689	2.197	Oxygenated cyclic
9	5-Methylfurfural	9.221	0.608	Furanic
10	2,5-Furandicarboxaldehyde	11.505	0.587	Furanic
11	Ethyl gallate	22.785	0.337	Phenolic/aromatic

*Relative peak area represents the percentage of the total chromatographic peak area assigned to each tentative annotation and should not be interpreted as absolute concentration. Compound assignments were based on comparison of mass spectra with library reference spectra. RT, retention time; GC–MS, gas chromatography–mass spectrometry.

Fatty acids constituted another major component of the annotated profile, with n-hexadecanoic acid and 9,12-octadecadienoic acid (Z,Z)- being particularly abundant. Octadecanoic acid and several fatty-acid esters were also detected. These compounds contribute to the overall chemical complexity of the extract but are not, on the basis of the present data, sufficient to explain the pH-dependent color response.

The GC–MS profile therefore demonstrates that the CAP-pretreated extract was chemically heterogeneous, with substantial contributions from phenolic/aromatic, furanic, and fatty-acid-related components. This complexity is important when interpreting the optical experiments because the color and UV–Vis response of the extract represents the combined behavior of multiple constituents rather than the response of a purified pigment system. Consequently, GC–MS is used here primarily to establish chemical context for the subsequent pH-dependent optical characterization rather than to assign the observed color changes to individual compounds.

3.3. pH-dependent color characteristics

The CAP-pretreated extract exhibited a pronounced and systematic pH-dependent change in its colorimetric characteristics (Figure 1). Across pH 2–12, substantial changes were observed in L*, a*, b*, chroma (C*), hue angle, and ΔE, demonstrating that the optical appearance of the extract was strongly influenced by the surrounding pH. Such pH-dependent color behavior is consistent with the well-established sensitivity of anthocyanin-containing systems to protonation and structural transformations. In Punica granatum var. pleniflora matrices, anthocyanins are important contributors to red coloration, and changes in anthocyanin composition or chemical environment are reflected in instrumental color parameters (Alighourchi and Barzegar 2009; Turfan et al. 2011).

The acidic region (pH 2–6) was characterized by relatively high L*, a*, b*, and C* values. Mean L* decreased progressively from 34.50 at pH 2 to 24.53 at pH 6, while a* decreased from 46.70 to 31.75 and b* from 41.83 to 31.58 over the same interval. Chroma similarly decreased from 62.69 to 44.78. These coordinated changes indicate a gradual modification of both lightness and chromatic intensity as the pH increased within the acidic range.

A more pronounced transition occurred around pH 7. At pH 7, L* decreased to 12.29, a* to 23.96, b* to 15.62, and C* to 28.60. Because pH 7 was selected as the reference condition for ΔE, its ΔE value was necessarily zero. Relative to this reference, the acidic samples exhibited substantial color differences, with ΔE values of 41.20, 32.95, 27.43, 21.85, and 21.56 at pH 2–6, respectively. These results demonstrate that the color differences between the acidic samples and the neutral reference were not merely instrumental fluctuations but represented pronounced changes in the overall CIELAB color space.

At pH 8–11, the extract remained within a relatively dark color regime, with L* values ranging from 10.34 to 11.67 and comparatively low a*, b*, and C* values. Although smaller fluctuations were observed among these pH values, the ΔE values remained distinguishable from the pH 7 reference, ranging from 2.54 to 6.06. This suggests that the optical state

established near neutral pH persisted across much of the moderately alkaline region, although the chromatic coordinates continued to vary.

A further distinct change occurred at pH 12. At this pH, L* decreased slightly to 10.16, while a* and b* decreased to 17.86 and 8.39, respectively, and C* decreased to 19.73. The resulting ΔE of 9.70 indicated a substantially different color state from the pH 7 reference. The distinct behavior at the strongly alkaline condition is chemically plausible because anthocyanin systems undergo additional transformations at alkaline pH, including formation and subsequent degradation of deprotonated quinonoidal and chalcone-related species. Anthocyanin color expression therefore cannot be interpreted solely as a simple reversible red-to-blue transition, particularly at higher pH where hydration, deprotonation, isomerization, and degradation processes may occur simultaneously (Pina 2014; Sousa et al. 2022).

The observed pH response is also consistent with previous studies of Punica granatum var. pleniflora products in which changes in anthocyanin content and instrumental color parameters were closely associated with changes in product quality and processing conditions. Punica granatum var. pleniflora color has been evaluated using L*, a*, b*, chroma, hue, and ΔE, demonstrating that instrumental color measurements provide a useful complementary description of pigment-related changes (Alighourchi and Barzegar 2009). Importantly, the present data extend this concept from monitoring color changes during storage or processing to deliberately characterizing the color response of a pomegranate-derived extract across a broad pH range.

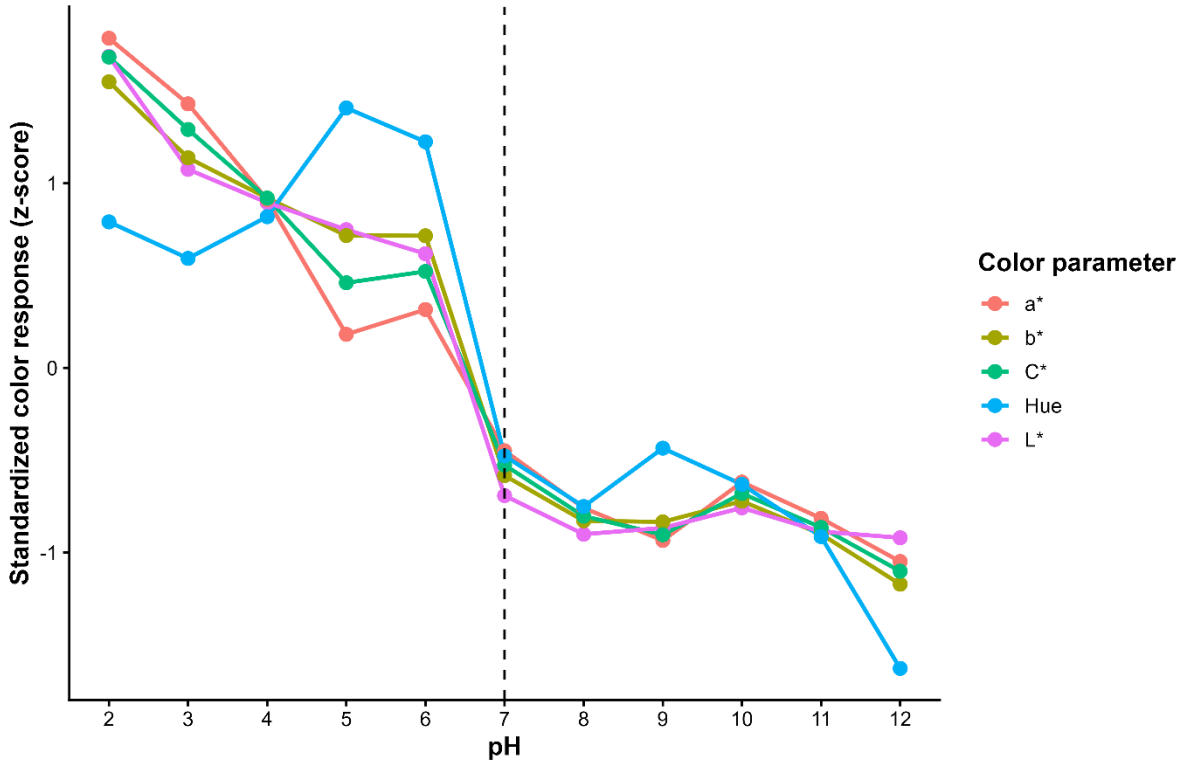


Figure 1. pH-dependent color characteristics of the CAP-pretreated *Punica granatum* var. *pleniflora* extract determined by digital image analysis.

The strong correlations among some of the color variables should, however, be interpreted with caution. L*, a*, and b* were strongly correlated, while C* and ΔE are mathematically derived from the underlying color coordinates. Therefore, these correlations primarily indicate a coordinated change in the CIELAB representation rather than independent biological relationships. For this reason, the subsequent multivariate analysis was based on a reduced set of non-redundant color and spectral variables.

The colorimetric results demonstrate that the CAP-pretreated extract possesses a pronounced and reproducible pH-responsive optical behavior. The particularly strong separation between the acidic region, the near-neutral/moderately alkaline region, and the strongly alkaline condition at pH 12 provided a clear basis for examining the corresponding changes in the UV–Vis absorption profile.

3.4. pH-dependent UV–Vis spectral behavior

The pH-dependent color changes were accompanied by substantial modifications in the visible absorption spectra of the CAP-pretreated extract (Figure 2). The UV–Vis measurements therefore provided an independent instrumental representation of the optical changes observed by CIELAB analysis. Because the spectra contained regions affected by detector saturation, interpretation was focused primarily on the visible region from 400 to 800 nm and on integrated spectral areas rather than on a simple comparison of individual maximum-absorbance wavelengths.

The integrated absorbance in the 450–550 nm region varied considerably with pH. The calculated areas were 139.52, 136.24, 96.81, 75.64, 86.39, 115.41, 108.60, 79.18, 108.16, 104.78, and 216.84 AU·nm for pH 2–12, respectively. The largest value occurred at pH 12, whereas the lowest value was observed at pH 5. This broad variation demonstrates that the pH-induced optical response was not restricted to a narrow spectral band but involved changes in the overall intensity and shape of the visible absorption profile.

Further separation of the visible spectrum into the 481–550 and 550–800 nm regions provided complementary information. The integrated area from 481 to 550 nm decreased from 98.12 AU·nm at pH 2 to 45.20 AU·nm at pH 5, followed by a partial recovery at pH 7 and additional fluctuations across the alkaline region. In contrast, the 550–800 nm area increased from 40.00 AU·nm at pH 2 to 60.75 AU·nm at pH 7 and reached 86.70 AU·nm at pH 12. The opposing behavior of these two spectral regions indicates that pH affected not only the magnitude of absorbance but also the distribution of spectral intensity across the visible region.

The spectral response is consistent with the established pH-dependent chemistry of anthocyanin-containing systems. Increasing pH can shift equilibria among differently protonated and hydrated anthocyanin forms, including flavylium cations, quinonoidal bases, hemiketal species, and chalcones. These transformations alter the electronic structure of the chromophores and consequently modify their visible absorption characteristics and perceived color (Pina 2014; Sousa et al. 2022). At strongly alkaline pH, additional degradation and

hydroxyl-dependent reactions may further modify the spectral response, making the behavior at pH 12 distinct from the response at moderately alkaline pH values.

The pH 12 spectrum was particularly distinctive, with an integrated 450–550 nm area of 216.84 AU·nm and a 550–800 nm area of 86.70 AU·nm. This strong spectral response agrees with the marked difference observed in the CIELAB coordinates at pH 12 and suggests that the strongly alkaline condition represents a distinct optical state rather than a simple continuation of the changes observed between pH 8 and 11.

A conservative approach to spectral interpretation was adopted because several wavelength regions approached or exceeded the instrumental saturation threshold. In particular, saturation was observed mainly in the approximately 428–476 nm region for pH 7, 8, 10, 11, and 12, with a much broader affected region at pH 12. Consequently, apparent shifts in individual spectral maxima in these regions may partly reflect detector saturation or boundary effects. Integrated spectral areas were therefore considered more robust descriptors of the pH-dependent response than a sequence of apparent λmax values.

The combined colorimetric and UV–Vis results demonstrate that the pH response observed visually and in CIELAB space was accompanied by measurable changes in the visible absorption profile. This agreement between two independent optical measurements supports the existence of a genuine pH-dependent optical response in the extract and provided the basis for subsequent multivariate integration of the color and spectral data.

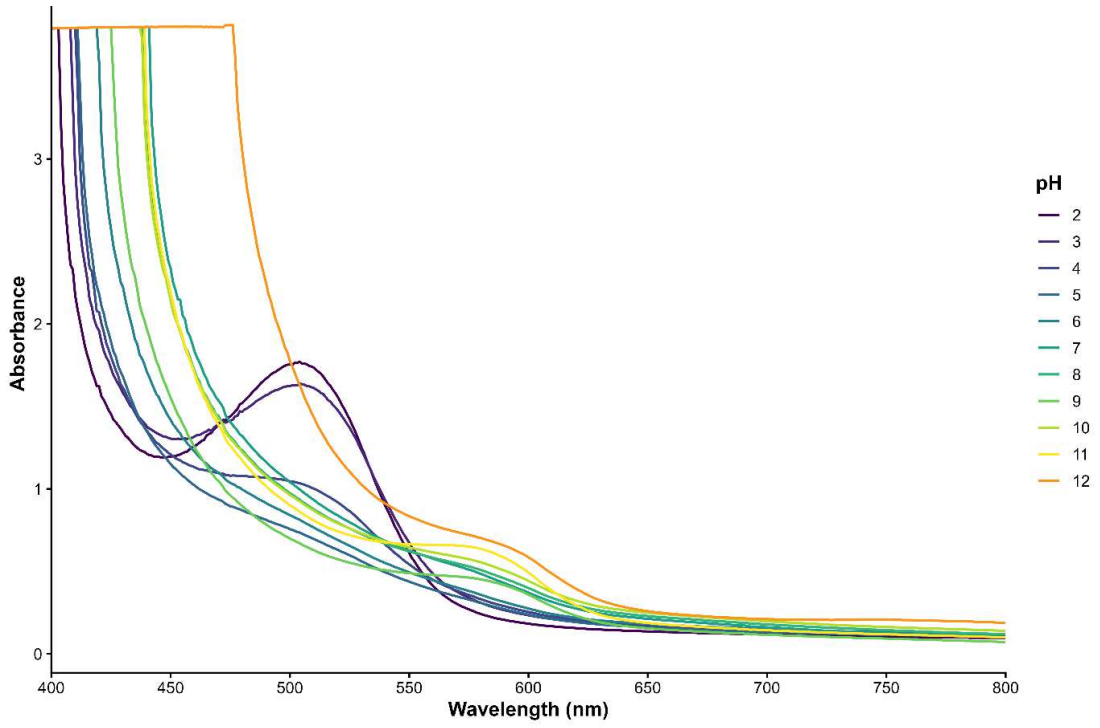


Figure 2. pH-dependent UV–Vis absorption spectra of the CAP-pretreated *Punica granatum* var. *pleniflora* extract in the visible region (400–800 nm). Spectra were recorded at pH 2–12 to characterize changes in the visible absorption profile associated with the pH-dependent color response.

3.5. Multivariate analysis of the integrated optical response

Principal component analysis (PCA) was applied to integrate the colorimetric and spectroscopic responses while avoiding excessive redundancy among mathematically related variables. The analysis included L*, a*, b*, hue angle, and the integrated UV–Vis areas from 481–550 and 550–800 nm. Chroma and ΔE were excluded because they are mathematically derived from the CIELAB coordinates, while the individual spectral PCA scores were excluded to avoid nesting derived variables within the integrated analysis.

The first two principal components accounted for 96.64% of the total standardized variance, with PC1 explaining 74.79% and PC2 explaining 21.85%. This high cumulative variance indicates that the major structure of the combined color–spectral dataset could be represented effectively in a two-dimensional space (Figure 3).

PC1 was strongly associated with the color coordinates. The loadings of L*, a*, and b* were −0.464, −0.450, and −0.469, respectively, while hue showed a loading of −0.433. The 550–800 nm spectral area also contributed substantially to PC1 (loading = +0.409). In contrast, the 481–550 nm area had only a small contribution to PC1 (loading = −0.082). Thus, PC1 primarily represented the coordinated variation of the main CIELAB color characteristics together with longer-wavelength visible absorbance.

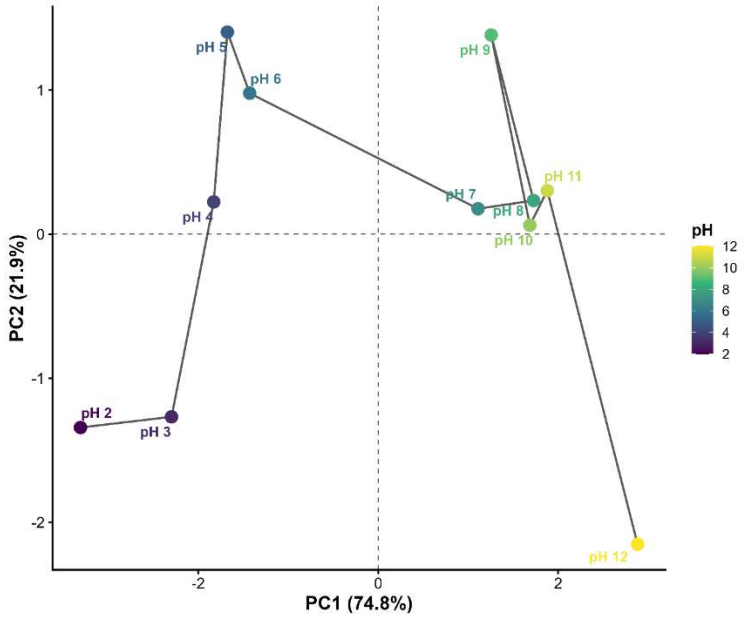


Figure 3. Principal component analysis of the integrated colorimetric and UV–Vis responses of the CAP-pretreated *Punica granatum* var. *pleniflora* extract across pH 2–12. PCA was performed using L*, a*, b*, hue angle, and integrated absorbance areas at 481–550 and 550–800 nm. The first two principal components explained 96.64% of the total variance.

PC2 was dominated by the 481–550 nm spectral area, which showed a loading of −0.855 and accounted for approximately 73.15% of the contribution to this component. The 550–800 nm area contributed less strongly (loading = −0.329), while hue made a moderate positive contribution (0.295). This indicates that PC2 captured spectral variation that was not fully represented by the general color-coordinate changes summarized by PC1.

The score distribution revealed a clear separation between the acidic pH region and the near-neutral/alkaline region. Samples from pH 2–6 had negative PC1 scores, ranging from −3.31 to −1.43, whereas pH 7–12 had positive PC1 scores ranging from 1.11 to 2.88. This separation demonstrates that the transition from acidic to neutral/alkaline conditions was the dominant source of variation in the combined optical dataset. The position of pH 12 was particularly distinctive, with a PC1 score of 2.88 and a PC2 score of −2.15, indicating that the strongly alkaline condition represented a substantially different optical state from the other pH levels.

The pH 4–6 samples were separated from the strongly acidic pH 2–3 samples mainly along PC2, reflecting changes in the 481–550 nm spectral region that were not fully explained by the general color-coordinate variation. Similarly, pH 9 occupied a relatively high positive PC2 position, indicating a distinct contribution from the shorter visible spectral region despite remaining within the broader alkaline cluster along PC1.

The PCA therefore provides an integrated representation of the pH-dependent optical response and confirms that the colorimetric and spectroscopic measurements contain complementary information. Rather than treating color and UV–Vis measurements as independent observations, the multivariate analysis demonstrates that they jointly describe a structured progression of optical states across the investigated pH range.

3.6. Integrated interpretation of color and spectral responses

The combined colorimetric and spectroscopic results indicate that the pH-dependent optical response of the CAP-pretreated extract was multidimensional rather than being represented by a single color parameter or absorption wavelength. This interpretation was supported by the correlations between the CIELAB variables and the integrated spectral regions. In particular, b* was strongly negatively correlated with the 550–800 nm spectral area (r = −0.808), while hue showed an even stronger negative correlation with this region (r = −0.864). These relationships indicate that changes in longer-wavelength visible absorption were closely associated with changes in the perceived chromatic characteristics of the extract.

In contrast, the 481–550 nm spectral area showed comparatively weak relationships with the color variables, with correlation coefficients of 0.307, 0.416, 0.239, and −0.178 with L*, a*, b*, and hue, respectively. This distinction is important because it demonstrates that the spectroscopic measurements were not simply redundant representations of the CIELAB measurements. Instead, the shorter visible spectral region captured additional variation that contributed strongly to PC2 in the integrated PCA.

The integrated PCA further confirmed this complementary behavior. PC1, which explained 74.79% of the total variance, was dominated by coordinated changes in L*, a*, b*, and hue together with the 550–800 nm spectral area, whereas PC2, explaining an additional 21.85%, was dominated by the 481–550 nm spectral area. Together, the two components accounted for 96.64% of the total variance. The resulting separation of acidic and neutral/alkaline samples and the distinct position of pH 12 demonstrate that the color and spectral measurements describe a coherent but multidimensional pH-response system.

The chemical profile obtained by GC–MS provides useful context for this optical behavior. The CAP-pretreated extract contained substantial phenolic/aromatic and furanic components in addition to fatty acids and other compounds. Phenolic constituents and anthocyanin-related compounds can participate in the optical properties of plant-derived matrices, while pH-dependent changes in anthocyanin protonation, hydration, deprotonation, and subsequent transformations can produce changes in both visible color and absorption behavior. However, the GC–MS results obtained in the present study do not establish which individual compound is responsible for any particular color coordinate or spectral region. This distinction is especially important because the extract represents a complex chemical matrix rather than a purified anthocyanin system.

The optical results should therefore be interpreted as a matrix-level pH response. The agreement among instrumental color measurements, visible absorption profiles, cross-domain correlations, and PCA provides stronger evidence for a systematic optical response than any single analytical parameter could provide independently. In particular, the consistent separation of acidic and neutral/alkaline conditions and the distinct behavior at pH 12 demonstrate that the response was structured across the entire pH range rather than being attributable to random variation.

Taken together, these findings demonstrate that the CAP-pretreated Punica granatum var. pleniflora extract exhibits a pronounced pH-responsive optical behavior that can be characterized using complementary colorimetric and UV–Vis measurements. GC–MS establishes the chemical complexity of the extract, colorimetry quantifies the macroscopic chromatic response, UV–Vis captures changes in visible absorption, and integrated PCA demonstrates the multivariate organization of these responses. This combined analytical framework provides a more comprehensive description of the optical behavior of the extract than would be obtained from color or spectroscopy alone and supports further consideration of the extract as a pH-responsive natural colorant or sensing material.

4. Conclusion

This study demonstrated that cold atmospheric plasma (CAP) pretreatment modified the chemical and functional characteristics of *Punica granatum* var. *pleniflora* peel extract and that the resulting extract exhibited a pronounced, systematic pH-dependent optical response. Comparison with the untreated control showed that CAP pretreatment altered extraction yield, antioxidant capacity, total phenolic content, and anthocyanin content in different directions, indicating modification rather than a uniform enhancement of extractability or functionality.

GC–MS analysis further revealed a chemically diverse profile comprising tentatively annotated phenolic/aromatic, furanic, fatty-acid, carbohydrate-related, and other oxygenated constituents. These annotations provide chemical context for the extract but do not establish compound-specific contributions to its optical properties. Digital image color analysis demonstrated distinct changes across pH 2–12, including a pronounced transition around neutral pH, a comparatively stable darker state under moderately alkaline conditions, and a further distinct response at pH 12. UV–Vis spectroscopy independently confirmed substantial redistribution of visible absorption across the same pH range. Integration of the colorimetric and spectral variables by PCA showed that the first two principal components accounted for 96.64% of the total variance, providing a concise multivariate representation of the pH-dependent optical response. The findings establish a coherent relationship between pH, color, and visible spectral behavior in the CAP-pretreated extract. The results support further investigation of this extract as a potential natural pH-responsive colorant or sensing component. However, practical application requires additional validation of color stability, reversibility, matrix effects, storage behavior, and performance in real food or packaging systems.

Acknowledgements

We express our gratitude to Golmakani, for her assistance in providing resources and technical guidance. Her contribution was instrumental in the successful completion of this research.

Funding Statement

The authors received no specific funding for this study.

Author Contributions

Mohammad Abdollahpour: Investigation, Methodology, Data curation. Farid Amidi-Fazli: Conceptualization, Methodology, Writing—original draft preparation, Reviewing, Validation, and Editing. Jalal Shayegh: Conceptualization, Methodology, Writing—original draft preparation, Reviewing, Validation, and Editing. Mehdi Gharekhani: Conceptualization, Methodology, Reviewing. Ali Rezapour: Conceptualization, Methodology, Reviewing. All authors reviewed the results and approved the final version of the manuscript.

Ethics Approval

Not applicable

Availability of Data and Materials

The authors confirm that the data supporting the findings of this study are available within the article.

Conflicts of Interest

The authors declare no conflicts of interest to report regarding the present study.

References

Ahmadian, S., Kenari, R. E., Amiri, Z. R., Sohbatzadeh, F., & Khodaparast, M. H. H. (2023). Effect of ultrasound-assisted cold plasma pretreatment on cell wall polysaccharides distribution and extraction of phenolic compounds from hyssop (Hyssopus officinalis

L.). *International Journal of Biological Macromolecules*, *233*(123557), 123557. https://doi.org/10.1016/j.ijbiomac.2023.123557

Ahmed, M., Zhang, H., & Xiong, Y. (2026). Anthocyanin structural types and stability: Implications for natural colorant applications in food systems. *Foods (Basel, Switzerland)*, *15*(12), 2080. https://doi.org/10.3390/foods15122080

Alashti, F. J., Sohbatzadeh, F., Ahmadian, S., Kenari, R. E., & Nazifi, E. (2023). Impact of atmospheric cold plasma pretreatment on morphology, structure, and chemical properties of clove (Syzygium aromaticum). *Lebensmittel-Wissenschaft und Technologie [Food Science and Technology]*, *191*(115639), Not Available. https://doi.org/10.1016/j.lwt.2023.115639

Alighourchi, H., & Barzegar, M. (2009). Some physicochemical characteristics and degradation kinetic of anthocyanin of reconstituted pomegranate juice during storage. *Journal of Food Engineering*, *90*(2), 179–185. https://doi.org/10.1016/j.jfoodeng.2008.06.019

Altaf, B., & Intipunya, P. (2026). Enhancing bioactive properties of butterfly pea (Clitoria ternatea) extract using cold atmospheric plasma and plasma-activated water while preserving color and total solids. *Innovative Food Science & Emerging Technologies*, *111*, 104606. https://doi.org/10.1016/j.ifset.2026.104606

Bao, Y., Reddivari, L., & Huang, J.-Y. (2020). Development of cold plasma pretreatment for improving phenolics extractability from tomato pomace. *Innovative Food Science & Emerging Technologies: IFSET: The Official Scientific Journal of the European Federation of Food Science and Technology*, *65*(102445), Not Available. https://doi.org/10.1016/j.ifset.2020.102445

Belwal, T., Dhyani, P., Bhatt, I. D., Rawal, R. S., & Pande, V. (2016). Optimization extraction conditions for improving phenolic content and antioxidant activity in Berberis asiatica fruits using response surface methodology (RSM). *Food Chemistry*, *207*, 115–124. https://doi.org/10.1016/j.foodchem.2016.03.081

Benzie, I. F. F., & Strain, J. J. (1996). The Ferric Reducing Ability of Plasma (FRAP) as a Measure of "Antioxidant Power": The FRAP Assay. *Analytical Biochemistry*, *239*(1), 70–76. https://doi.org/10.1006/abio.1996.0292

Bursać Kovačević, D., Putnik, P., Dragović-Uzelac, V., Pedisić, S., Režek Jambrak, A., & Herceg, Z. (2016). Effects of cold atmospheric gas phase plasma on anthocyanins and color in pomegranate juice. *Food Chemistry*, *190*, 317–323. https://doi.org/10.1016/j.foodchem.2015.05.099

Chang, C. C., Yang, M. H., Wen, H. M., & Chern J.C. (2002). Chang_flavonoids_PDF. *J. Food Drug Anal*, (10), 178–182.

Cheng, J., Li, J., Xiong, R.-G., Wu, S.-X., Huang, S.-Y., Zhou, D.-D., et al. (2023). Bioactive compounds and health benefits of pomegranate: An updated narrative review. *Food Bioscience*, *53*(102629), 102629. https://doi.org/10.1016/j.fbio.2023.102629

Fischer, U. A., Carle, R., & Kammerer, D. R. (2013). Thermal stability of anthocyanins and colourless phenolics in pomegranate (Punica granatum L.) juices and model solutions. *Food Chemistry*, *138*(2–3), 1800–1809. https://doi.org/10.1016/j.foodchem.2012.10.072

Fontana, A., Rodríguez, I., & Cela, R. (2018). Dispersive liquid-liquid microextraction and gas chromatography accurate mass spectrometry for extraction and non-targeted profiling of volatile and semi-volatile compounds in grape marc distillates. *Journal of Chromatography A*, *1546*, 36–45. https://doi.org/10.1016/j.chroma.2018.03.003

Ghasemi-Nezhad, L., Goli, S. A. H., & Soleimanian-Zad, S. (2025). Improving phenolics extractability from pomegranate seed meal applying roasting and cold plasma pretreatment; their application in mayonnaise as antioxidant and antimicrobial agents. *Applied Food Research*, *5*(1), 101050. https://doi.org/10.1016/j.afres.2025.101050

Herceg, Z., Kovačević, D. B., Kljusurić, J. G., Jambrak, A. R., Zorić, Z., & Dragović-Uzelac, V. (2016). Gas phase plasma impact on phenolic compounds in pomegranate juice. *Food Chemistry*, *190*, 665–672. https://doi.org/10.1016/j.foodchem.2015.05.135

Heydari, M., Carbone, K., Gervasi, F., Parandi, E., Rouhi, M., Rostami, O., et al. (2023). Cold plasma-assisted extraction of phytochemicals: A review. *Foods (Basel, Switzerland)*, *12*(17), 3181. https://doi.org/10.3390/foods12173181

Keshavarzi, M., Najafi, G., Ahmadi Gavlighi, H., Seyfi, P., & Ghomi, H. (2020). Enhancement of polyphenolic content extraction rate with maximal antioxidant activity from green tea leaves by cold plasma. *Journal of Food Science*, *85*(10), 3415–3422. https://doi.org/10.1111/1750-3841.15448

Khalili, M., Najafi, A., & Razavi, R. (2025). Preservative activity of free and nano-encapsulated pomegranate peel extract obtained using cold plasma and ultrasound-assisted method in increasing the shelf life of thigh mutton mince. *Applied Food Research*, *5*(1). https://doi.org/10.1016/j.afres.2024.100668

Kumar, S., Singh, P., & Kumar, D. (2024). Comprehensive volatile composition of vegetative parts of Bunium persicum B. Fedtsch.: Spice of alpine Himalaya. *Journal of Biologically Active Products From Nature*, *14*(2), 187–198. https://doi.org/10.1080/22311866.2024.2307560

Kyriakoudi, A., Loukri, A., Christaki, S., Oliinychenko, Y., Stratakos, A. C., & Mourtzinos, I. (2024). Impact of cold atmospheric plasma pretreatment on the recovery of phenolic antioxidants from spent coffee grounds. *Food Analytical Methods*, *17*(10), 1484–1496. https://doi.org/10.1007/s12161-024-02661-2

Maqsood, M., Saeed, R. A., Rahman, H. U. U., Khan, M. I., & Khalid, N. (2025). Pomegranate punicalagin: A comprehensive review of various in vitro and in vivo biological studies. *ACS Food Science & Technology*, *5*(6), 2064–2085. https://doi.org/10.1021/acsfoodscitech.5c00117

Pina, F. (2014). Chemical applications of anthocyanins and related compounds. A source of bioinspiration. *Journal of Agricultural and Food Chemistry*, *62*(29), 6885–6897. https://doi.org/10.1021/jf404869m

Razazian, G., Dalvi-Isfahan, M., & Mohtashami, S. (2026). Lime peel as an industrial resource: Improving the extraction efficiency of volatiles and polyphenols via cold plasma. *Applied Food Research*, *6*(1), 101738. https://doi.org/10.1016/j.afres.2026.101738

Reisdorph, N. A., Walmsley, S., & Reisdorph, R. (2019). A perspective and framework for developing sample type specific databases for LC/MS-based clinical metabolomics. *Metabolites*, *10*(1), E8. https://doi.org/10.3390/metabo10010008

Salim, A., Deiana, P., Fancello, F., Molinu, M. G., Santona, M., & Zara, S. (2023). Antimicrobial and antibiofilm activities of pomegranate peel phenolic compounds: Varietal screening through a multivariate approach. *Journal of Bioresources and Bioproducts*, *8*(2), 146–161. https://doi.org/10.1016/j.jobab.2023.01.006

Shimada, Kazuko., Fujikawa, Kuniko., Yahara, Keiko., & Nakamura, Takashi. (1992). Antioxidative properties of xanthan on the autoxidation of soybean oil in cyclodextrin

emulsion. *Journal of Agricultural and Food Chemistry*, *40*(6), 945–948. https://doi.org/10.1021/jf00018a005

Shu, P., Qing, Y., Sheng, J., Yao, X., Zhang, Z., & Shen, L. (2026). Integrated analysis of metabolomics and transcriptomics reveals potential transcription factors regulating anthocyanin synthesis in pomegranate fruit. *Scientia horticulturae*, *355*(114570), 114570. https://doi.org/10.1016/j.scienta.2025.114570

Singleton, V. L., & Rossi, J. A. (1965). Colorimetry of Total Phenolics with Phosphomolybdic-Phosphotungstic Acid Reagents. *American Journal of Enology and Viticulture*, *16*(3), 144–158. https://doi.org/10.5344/ajev.1965.16.3.144

Sousa, D., Basílio, N., Oliveira, J., de Freitas, V., & Pina, F. (2022). A new insight into the degradation of anthocyanins: Reversible versus the irreversible chemical processes. *Journal of Agricultural and Food Chemistry*, *70*(2), 656–668. https://doi.org/10.1021/acs.jafc.1c06521

Sun, L., Shi, F., He, X., Cai, Y., Yu, Y., Yao, D., et al. (2023). Establishment and application of quantitative method for 22 organic acids in honey based on SPE-GC–MS. *Zeitschrift für Lebensmittel-Untersuchung und -Forschung. A [European Food Research and Technology]*, *249*(2), 473–484. https://doi.org/10.1007/s00217-022-04146-0

Turfan, Ã., TÃ¼rkyÄ±lmaz, M., YemiÅ□, O., & Ã□zkan, M. (2011). Anthocyanin and colour changes during processing of pomegranate (Punica granatum L., cv. Hicaznar) juice from sacs and whole fruit. *Food Chemistry*, *129*(4), 1644–1651. https://doi.org/10.1016/j.foodchem.2011.06.024

Yang, Z., Zhai, X., Zou, X., Shi, J., Huang, X., Li, Z., et al. (2021). Bilayer pH-sensitive colorimetric films with light-blocking ability and electrochemical writing property: Application in monitoring crucian spoilage in smart packaging. *Food Chemistry*, *336*, 127634. https://doi.org/10.1016/j.foodchem.2020.127634

Zhang, M., Tang, X., Mao, B., Zhang, Q., Zhao, J., Chen, W., & Cui, S. (2025). Pomegranate: A comprehensive review of functional components, health benefits, processing, food applications, and food safety. *Journal of Agricultural and Food Chemistry*, *73*(10), 5649–5665. https://doi.org/10.1021/acs.jafc.4c05428

Zulfiqar, M., Gadelha, L., Steinbeck, C., Sorokina, M., & Peters, K. (2023). MAW: the reproducible Metabolome Annotation Workflow for untargeted tandem mass spectrometry. *Journal of Cheminformatics*, *15*(1), 32. https://doi.org/10.1186/s13321-023-00695-y

Supplementary Files

This is a list of supplementary files associated with this preprint. Click to download.

- supplementary.docx
- graphicalabstract.png